



Contents lists available at ScienceDirect

Journal of the European Ceramic Society

journal homepage: www.elsevier.com/locate/jeurceramsoc

High-capacity $\text{Li}_4\text{Ti}_5\text{O}_{12}$ -C thick ceramic electrodes manufactured by powder injection moulding

I. Romero-Garcia^a, M.E. Sotomayor^a, B. Levenfeld^a, A. Varez^{a,*}, A. Varzi^{b,c}, G.T. Kim^{b,c}, S. Passerini^{b,c,d}

^a Department of Materials Science and Engineering and Chemical Engineering, Universidad Carlos III de Madrid, Leganes, 28911 Madrid, Spain

^b Helmholtz Institute Ulm (HIU), Helmholtzstrasse 11, 89081 Ulm, Germany

^c Karlsruhe Institute of Technology (KIT), P.O. Box 3640, 76021 Karlsruhe, Germany

^d Department of Chemistry, Sapienza University of Rome, Piazzale A. Moro 5, 00185 Rome, Italy

ARTICLE INFO

Keywords:

Powder injection moulding
Binder-free electrodes
Thick electrodes
High volumetric energy density
Li-ion battery

ABSTRACT

Lithium-ion batteries are the most efficient electrochemical energy storage devices. However, there is still room for improvement in terms of safety and energy density, presently limited by conventional tape-casting electrode processing. In this study, a blend of the anodic material $\text{Li}_4\text{Ti}_5\text{O}_{12}$ with 2 wt% carbon black has been processed through powder injection moulding (PIM) yielding, after subsequent debinding and sintering processes, to ultrathick (>500 μm) ceramic binder-free electrodes. The mixture of $\text{Li}_4\text{Ti}_5\text{O}_{12}$ with the thermoplastic binder composed of polypropylene, paraffin wax, and stearic acid is investigated to identify a rheologically suitable feedstock for the PIM process. The resulting disk-type green parts contain 50 vol% of ceramic powder. After removing the binder with solvents and subsequent thermal treatment, the parts are sintered at 900 °C, aiming for a relatively high porosity, i.e., 25.7%. The resulting electrodes show very high areal and volumetric capacities up to 26.0 $\text{mA}\cdot\text{h}\cdot\text{cm}^{-2}$ and 403 $\text{mA}\cdot\text{h}\cdot\text{cm}^{-3}$ at C/24, respectively, in a half-cell against lithium metal.

1. Introduction

Lithium-ion batteries (LIBs) have become indispensable in the modern Society, being used in small-scale applications linked to consumer electronics, such as mobile phones and laptops, as well as large-scale applications such as electric vehicles and microgrids, due to their high energy density and long cycle life [1,2]. LIBs were first commercially produced in 1991 by Sony Inc. using LiCoO_2 as cathode, petroleum coke (soft carbon) as anode and LiPF_6 in propylene (PC) as electrolyte. The development of new cathode, anode and electrolyte materials has improved the energy density and reduced the cost, but the essence of LIBs has not changed much since their discovery [1–3]. Typically, the electrode manufacturing of commercial batteries involves four main steps [4]: 1) *slurry mixing*, where the active materials, conductive agents and polymeric binders are mixed with solvents to obtain homogeneous slurries; 2) *coating* of current collectors with the slurries; 3) *drying* of the electrodes by heating to adequately remove the solvent and, finally, 4) *calendaring*, in which the film is compressed by two metal rollers to a suitable thickness with uniform porosity. This technology often requires

the use of toxic organic solvents such as N-methylpyrrolidone (NMP), which can harm humans and the environment, including the reproductive system, eyes, skin and respiratory system [5,6]. Furthermore, the removal of this solvent, with its high boiling temperature (202 °C), significantly increases the cost of the manufacturing process. The presence of non-active materials (binders, solvent, and conductive agents) is necessary in this manufacturing process and reduces the total specific capacity of the cell. Moreover, this process inherently imposes a limitation on the thickness of the electrodes typically restricted to a few dozen of microns [7].

With the aim of reducing the amount of non-active components and increasing the thickness of the electrodes, we have recently demonstrated the feasibility of the Powder Extrusion Moulding (PEM) process for the manufacturing of thick ceramic electrodes (500–1000 μm) for lithium-ion battery applications [8,9]. The electrodes consist only of active material because the binder can be removed from them, which, along with their thickness, increases considerably the areal and volumetric capacities of the cell. Moreover, these binder-free electrodes greatly facilitate their recycling. All these features are an added value to

* Correspondence to: Department of Materials Science and Engineering and Chemical Engineering, Universidad Carlos III de Madrid, Avda. Universidad, 30, Leganes, 28911 Madrid, Spain.

E-mail address: alvar@ing.uc3m.es (A. Varez).

<https://doi.org/10.1016/j.jeurceramsoc.2023.09.030>

Received 6 August 2023; Received in revised form 6 September 2023; Accepted 12 September 2023

Available online 13 September 2023

0955-2219/© 2023 The Authors. Published by Elsevier Ltd. This is an open access article under the CC BY-NC-ND license (<http://creativecommons.org/licenses/by-nc-nd/4.0/>).

this technology as the additives and, above all, the current collectors increase the weight of the battery and the difficulty in their disposal.

The search for alternative electrode processing routes is the main motivation of this work, which describes the application of Powder Injection Moulding (PIM) to the manufacturing of LTO ceramic thick electrodes for LIBs. This processing method, quite similar to PEM, combines traditional plastic injection moulding with ceramic technology in order to obtain complex shape ceramic pieces [10]. Briefly, the process starts with mixing the ceramic powder with a multicomponent binder system to produce the feedstocks with adequate viscosity. Subsequently, and after pelletizing the feedstock, the injections process takes place producing the so-called “green parts” with the shape of the desired final part. After, a de-binding step is required to remove the polymer, which results in fragile “brown” parts. A controlled sintering process yields the final pieces, whose geometry can be as diverse as the design of the mould of the injection machine. Generally, PIM is suitable for producing small, complex pieces, that can achieve very high densities with good dimensional precision (Tolerances are between $\pm 0.1\%$ and $\pm 0.5\%$ of dimension), and with high production rates [11–13]. This technology has been widely used for structural materials (metals and ceramics). Within the electrochemistry field, there are precedents of its use for solid oxide fuel cells [14–16] but not for LIBs.

The lithium titanate spinel, $\text{Li}_4\text{Ti}_5\text{O}_{12}$ (LTO), is a well-known negative electrode material, which can insert up to three lithium ions varying its lattice parameter from 8.3595 Å to 8.3538 Å. This results in a volumetric change of barely 0.2% (i.e., zero-strain material); and, thus, great cyclability [17,18]. Due to the relatively high equilibrium voltage, 1.55 V against the couple Li/Li^+ , it has been proposed that the formation of the solid-electrolyte interphase (SEI) resulting from the electrolyte solvent and salt decomposition does not occur, avoiding the Li^+ ion inventory loss occurring, e.g., with graphite [19]. The low reactivity of lithiated LTO makes it a much safer anode material compared to conventional graphite [20]. Additionally, it offers a decent specific capacity of $175 \text{ mA}\cdot\text{h}\cdot\text{g}^{-1}$, but its main drawback is its low electric conductivity, down to $10^{-13} \text{ S}\cdot\text{cm}^{-1}$, related to the high oxidation state of titanium [17]. Although in some works it is claimed that a relatively small lithiation extent is sufficient to increase the electronic conductivity of LTO by several orders of magnitude [19,21], several manuscripts report on different strategies to increase the charge transfer reaction rate by either ion doping—promoting a partial substitution of Ti^{4+} with Ti^{3+} [22, 23]—or conductive carbon addition. This last approach can be done by mixing the LTO with carbon particles or coating the ceramic particles with a thin carbon layer via, e.g., thermal treatment of different organic carbon sources, such as citric acid [24], toluene [25] or activated carbon from coconut shells [26]. The straightforward mix, despite its carbon distribution not being as homogeneous, has the advantage of not fully covering the ceramic grains, therefore not hindering the lithium exchange at the active material surface exposed to the between electrolyte [17]. This present study focuses on the latter approach.

The aim of this work was to obtain binder-free, thick $\text{Li}_4\text{Ti}_5\text{O}_{12}$ (LTO) electrodes for LIBs by powder injection moulding. Due to the insulating character of sintered LTO, conductive carbon black Super C65 (2% of the total weight) was added. The various steps of the processing were optimised, and the sintered parts obtained were characterised with different physical and chemical techniques. Finally, electrochemical characterization in pouch bag cells (lithium used as the counter electrode) was carried out to determine their suitability as LIB electrodes.

2. Materials and methods

2.1. Materials

A commercially available $\text{Li}_4\text{Ti}_5\text{O}_{12}$ (LTO) powder (Linyi Gelon Lib Co., China) was employed as the active material. According to the manufacturer, the particle size distribution comprehends d_{10} , d_{50} , and d_{90} values of 0.2, 1.0, and 3.0 μm , respectively. The particles are slightly

aggregated and have an irregular shape as it can be seen in Fig. 1a. The pycnometric density (measured with a Micromeritics AccuPyc 1330, USA) is $3.533 \pm 0.004 \text{ g}\cdot\text{cm}^{-3}$. Another ceramic component of the feedstock is a conductive carbon black Super C65 (C) (Imerys, Switzerland), with a pycnometric density of $1.92 \pm 0.01 \text{ g}\cdot\text{cm}^{-3}$. The electrodes were designed to contain 2 wt% of carbon black.

The binder system is a multicomponent mixture constituted by polypropylene (PP) (Repsol, Spain) as the polymeric backbone; paraffin wax (PW) (PanReac AppliChem, Spain) to reduce the viscosity of the mixture; and stearic acid (SA) (PanReac AppliChem, Spain) as a surfactant. This system was already and successfully used in our research group for PIM and PEM processing of different ceramic materials [8,14].

2.2. Feedstock preparation and rheological study

The volumetric proportion of PP, PW, and SA was 50:46:4. Firstly, the critical powder volume percentage (CPVP) was estimated through torque measurements of the different powder-binder mixtures (feedstock). The preparation of the feedstock was carried out through various steps:

- 1) Before the mixing step, a mixture of LTO, C and SA was prepared. Firstly, the SA was quickly dissolved in an exceeding volume of ethanol 96%. Secondly, a dispersion of the ceramic powders was made with an Ultra-Turrax Micra D9 (Germany) operating at 11,000 rpm. The LTO powder was added gradually into the ethanol and, afterwards, the carbon black as well. The resulting mixture was homogenised for 15 min. Lastly, the suspension was placed in an oven at 50 °C for 24 h, and a grey powder was obtained. After preparation of the premix with C and SA, carbonaceous matter may be present (Fig. 1b).
- 2) This powder and the other components of the binder were mixed in a Haake Rheocord 252p (Germany) mixer with dual rotor blades, at 40 rpm and 180 °C for 40 min.
- 3) Lastly, the solidified feedstock was milled in a Retsch SM 100 device (Germany) to obtain grains with a diameter of less than 0.5 mm, which have a more suitable size for the injection machine.

Six different formulations of ceramic powder (LTO+C) loading were prepared to investigate the optimal feedstock composition: 50, 51, 52.5, 55, 56.5 and 58 vol%.

Rheological studies were performed by applying shear rates between 100 and $10,000 \text{ s}^{-1}$ at 170, 180 and 190 °C. The instrument employed was a Haake Rheocap S20 (Germany) capillary rheometer whose die had dimensions of 30 mm length (L), and 1 mm diameter (D) (L/D ratio of 30).

2.3. Injection moulding process (green part preparation)

Larger quantities of the optimised mixture were processed in the injection machine (Arburg 220 S 250–60, Germany) obtaining disk-type pieces from a 12 mm \times 0.7 mm mould. With an established maximum injection pressure of 1000 bar, optimization of the process was carried out by varying the injection volume and other parameters to obtain high dense and defects-free pieces. The optimised parameters for the injection process are shown in Table 1.

2.4. Debinding and sintering processes

Binder removal was performed by a combination of solvent and thermal debinding, resulting in the so-called brown pieces. In the first step, i.e., solvent debinding, PW and SA are removed by solubilization in n-heptane 50 °C. The thermal debinding (Goceram GCDV 50/2, Sweden) was done by heating at a rate of $5 \text{ }^\circ\text{C}\cdot\text{min}^{-1}$ to 200 °C, 30 min plateau, then heating at $1 \text{ }^\circ\text{C}\cdot\text{min}^{-1}$ up to 450 °C, 60 min plateau and, finally, cooling down to room temperature at $5 \text{ }^\circ\text{C}\cdot\text{min}^{-1}$ (Fig. S1). The

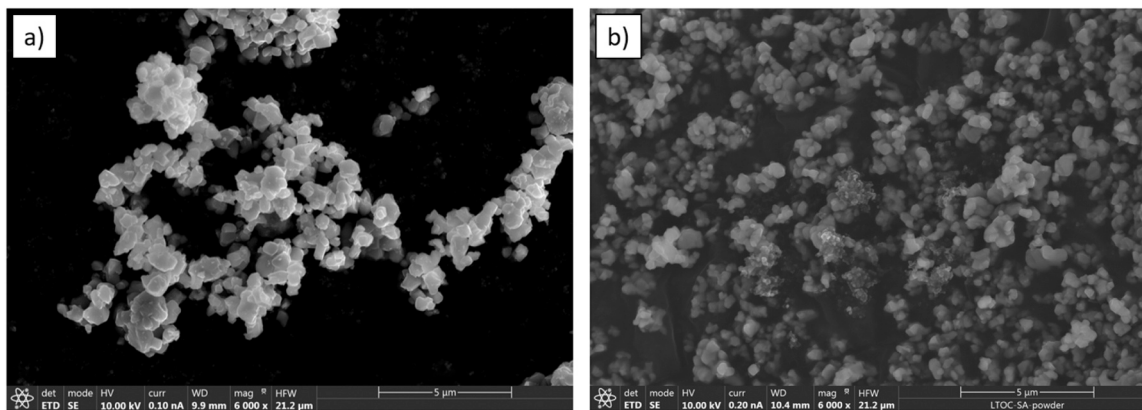


Fig. 1. SEM micrographs of a) the pristine LTO powder, b) the mixture of powders composed of LTO, carbon black and stearic acid.

Table 1
Injection moulding parameters.

Injection cylinder temperature gradient (°C)	170/175/180/185
Mould temperature (°C)	50
Dosing volume (cm ³)	10
Commuting point (cm ³)	7.6
Flow (cm ³ ·s ⁻¹)	35
Maximum pressure (bar)	1000
Post-pressure profile	600 bar 0.4 s 200 bar 0.2 s
Cooldown time (s)	20

gas used was a mixture of Ar/H₂ (5 vol%) at a pressure of 2 bar. The same atmosphere was used in the sintering step (Carbolite CTF 18/300, UK) where the samples were heated at 900 °C, with a constant heating rate of 2 °C·min⁻¹, for one hour (Fig. S1).

2.5. Characterization

The density of the LTO/C sintered pieces was measured through the Archimedes method, employing an acrylic lacquer as a sealing agent. Ten samples were measured and the average value is given besides the standard deviation. X-ray diffraction (XRD) analysis was performed in a Philips X'Pert (Netherlands) diffractometer with a (θ/2θ) Bragg–Brentano geometry, employing Cu-K_α radiation. The 2θ range analysed was 10–90° with a step scan of 0.02° and a counting time of 8 s per step. Carbon content of the samples was determined by elemental analysis, using a LECO CS-200 (USA) analyser. Differential scanning calorimetry (DSC) analysis (Perkin Elmer Diamond, USA) was employed to verify the full elimination of PW and SA during the solvent debinding step. The experiments were done with N₂ as the working atmosphere from 0° to 200°C with a heating rate of 10 °C·min⁻¹.

The microstructure of the powders and the different samples were studied by scanning electron microscopy (SEM), with an FEI Teneo (USA) working at 10 kV. Moreover, transmission electron microscopy (TEM) of sintered samples was performed, using a JEOL JEM 300 F (Japan) microscope operating at 300 kV.

Electrochemical impedance spectroscopy (EIS) studies were performed in a Solartron 1260 (UK) analyser, on a range between 0.1 Hz and 10⁶ Hz, with an amplitude sinusoidal wave perturbation of 100 mV. Prior to the measurements, gold ion-blocking electrodes were painted on both sides of the pellets, and they were set at 750 °C for thirty minutes in the same atmosphere of the sintering (Fig. S1).

2.6. Electrochemical characterization (battery behaviour)

Further electrochemical characterization of the LTO/C electrodes was done by studying the battery behaviour in pouch-bag cells, using

lithium foils (Sigma-Aldrich, Germany) as the counter-electrode. The LTO/C electrodes were coated on one side with a gold paint to act as current collector, which was subjected to the same thermal treatment as described for EIS. In these cells, a Hipore SV718 separator (Asahi Kasei, Japan) was employed, and 1 mL of liquid electrolyte LP30 (1 M LiPF₆ in a mixture of the same volume of EC and DMC, supplied by Sigma-Aldrich, Germany) was added. This large amount of electrolyte is enough to fill all the open pores of the electrode. The cell was assembled in a dry room whose dew point was below – 65 °C. The electrochemical cycling tests were carried out with a Maccor (USA) series 4000 potentiostat, at 20 ± 1 °C in the voltage range between 1 and 2 V. The C rates were C/24 for the first and second cycles, and from then on C/12, being 1 C = 175 mA·g⁻¹.

3. Results and discussion

3.1. Powder loading analysis

The feedstock was produced in the rotor blade mixer by adding the mixture of LTO, SuperC65 and SA to the binder system (paraffin wax and polypropylene). This operation was performed while keeping the torque value under control before adding more ceramic powder to the mixing chamber. The variations of torque with mixing time for each feedstock are depicted in Fig. 2a. First, the binder components (PP and PW) are introduced into mixing chamber and then small portions of the mixture of powders were added until the torque was stabilised. It can be seen how, for the different feedstocks, the powder additions cause an increase in the torque value. After the last powder addition, the steady state value associated with the homogenization of the ceramic-polymer mixtures is reached. In general, the mixing time to reach steady-state torque τ , was less than 10 min, which indicates the good homogeneity of these systems. Nevertheless, the 56.5% and 58% feedstocks were hardly forming a uniform mixture, as it can be seen in their noisier curves. The values of τ were taken by averaging the data of the last five minutes of mixing, as in that interval the torque did not fluctuate significantly. It is observed that for powder loading between 50% and 55%, the steady-state torque is about 1 N·m, but there is a noticeable increment for 56.5% and 58%. In comparison to prior findings [8] on carbon black-free LTO (Fig. 2b), torque values present a similar trend. Notably, the incorporation of carbon black into LTO powder complicates the mixing process provoking higher torque. The critical powder volume concentration (CPVC), determined by the slope change in torque curves [27] is slightly shifted towards higher powder loading (52.5% for LTO and to 55% for LTO/C).

3.2. Feedstock rheology

Flow behaviour of the feedstock is very important to determine the suitability of the mixture to be injected. Feedstocks should have good

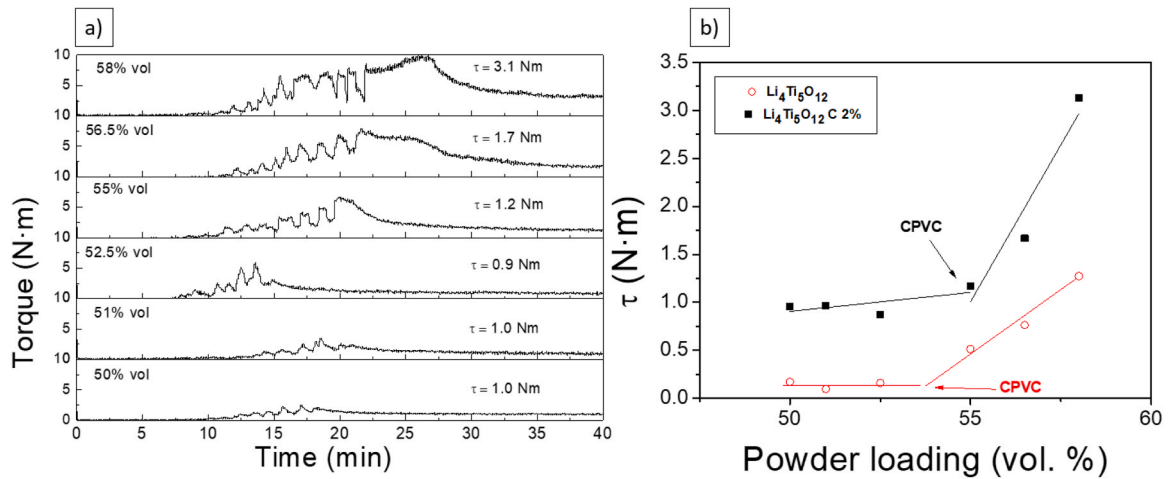


Fig. 2. a) Mixing torque vs time for each composition, noted in powder volumetric charge. The steady-state torque is written at the right of every graph, b) comparison of steady-state torque variation towards powder volumetric charge for LTO samples with and without conductive carbon black.

stability and relatively low viscosity, below 1000 Pa·s in the 100–2000 s⁻¹ shear rates interval [28]. The rheological properties of the prepared feedstock were evaluated through capillary rheology. For the sake of comparison with the other identical feedstock without conductive carbon black [8], tests were performed on samples with powder loading of 50 and 55 vol%. Fig. 3 shows the variation of the viscosity with the shear rate at 170, 180 and 190 °C for the feedstocks with different powder loadings. According to the pseudoplastic characteristics of the binder system, the viscosity decreases as the shear rate increases. This behaviour is the most suitable for the injection moulding process, as it assures uniform filling of the mould. The greater the LTO/C powder loading, the bigger the values of viscosity obtained, which is coherent with the previous pattern of steady-state torque. Meanwhile, the inverse happens with the temperature at which the test is done. The pseudoplastic behaviour ($n < 1$) can be quantified by determining the flow index value, n , in the Ostwald and De Waele law [29,30] (Table 2):

Table 2
Flow behaviour index for the feedstocks at different temperatures.

Powder loading (%vol)	n			Activation Energy 1000 s ⁻¹ (kJ·mol ⁻¹)
	170 °C	180 °C	190 °C	
50	0.59	0.60	0.63	41.2
55	0.55	0.57	0.61	42.3

$$\tau = k \cdot \dot{\gamma}^n$$

where τ is the shear stress, k is the flow consistency index, $\dot{\gamma}$ is the shear rate and n is the flow behaviour index.

For the LTO/C feedstocks, it is observed that n increases slightly with the temperature, effect previously reported on LTO without C [8].

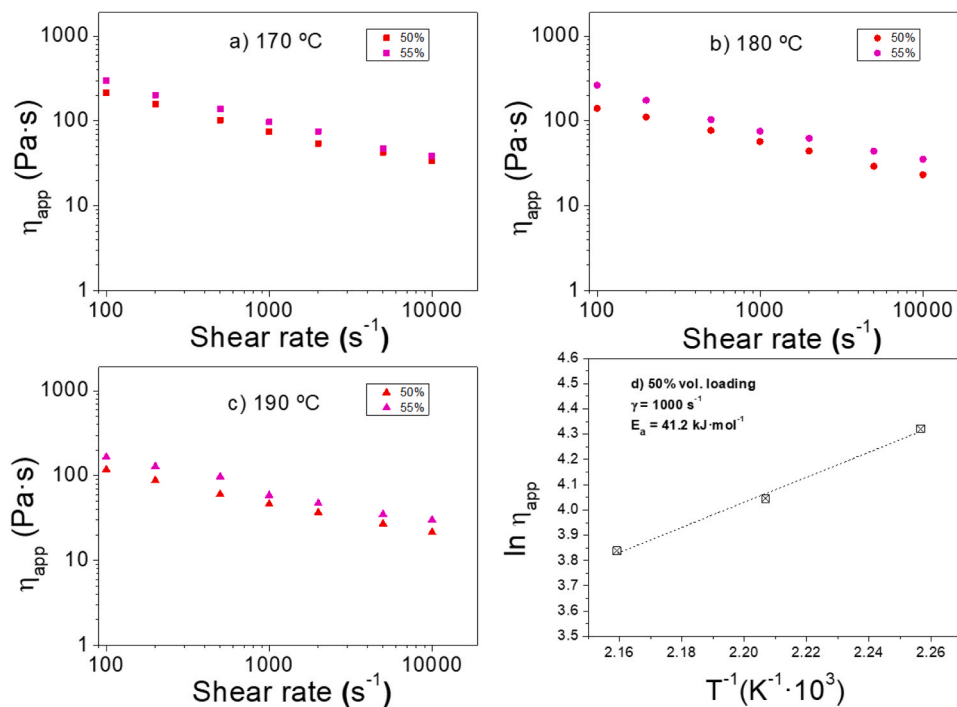


Fig. 3. Rheological tests for 50% and 55% powder loading feedstocks of LTO/C at temperatures: a) 170 °C, b) 180 °C, and c) 190 °C. d) Example graph of an Arrhenius representation to obtain the activation energy of the flow of the feedstock.

Similarly to other reports for the same binding system [8,31], a pattern of decreasing n with higher powder loading is also appreciated.

Fig. 3 depicts that higher powder loading corresponds to increased viscosity. Working with a highly viscous feedstock provokes challenges in terms of injection machine operation such as possible jamming and inadequate canal filling. Considering the requirement for a high porosity thick electrode, a decision was made to proceed with the PIM process using the feedstock constituted of 50% of powder loading. In Fig. 3d), an Arrhenius representation for the calculation of the activation energy of the flow of this feedstock is presented. The dependence between viscosity and temperature according to this model follows this equation:

$$\eta = \eta_0 \cdot e^{\frac{E_a}{RT}}$$

η is the viscosity, η_0 is the viscosity at a reference temperature T_0 , R is the ideal gas constant, T is the temperature and E_a is the flow activation energy.

The data are applied for a shear rate of 1000 s^{-1} , which is representative of the flow in a ceramic injection moulding process according to Edirishinge and Evans [32]. The activation energy of $41.2 \text{ kJ}\cdot\text{mol}^{-1}$ for 50% powder loading is relatively high, but in the range of other feedstocks used for PIM purpose. With greater powder loading, the activation energy slightly increases to $42.3 \text{ kJ}\cdot\text{mol}^{-1}$, this rather small dependence may be related to the fact that the loading is not too far from the CPVC.

To understand the influence of carbon black on the viscosity of the feedstock, further rheological tests were performed on an identical carbon-free LTO feedstock (Fig. 4). The presence of the carbon black has a notable influence on the mixture, as can be appreciated by the fact that the viscosity is greater for LTO/C, varying from 15.28 to $57.07 \text{ Pa}\cdot\text{s}$ for the $180 \text{ }^\circ\text{C}$, 1000 s^{-1} measurement. Moreover, the graphics depict an influence of temperature considerably lower for the latter, confirmed with the flow activation energy value for the sample LTO 50% ($12.4 \text{ kJ}\cdot\text{mol}^{-1}$) [8].

3.3. Injection process

Based on the rheological results, the injection process was performed with the feedstock containing a 50% vol. charge of LTO/C. In this step, several parameters are optimised to obtain defect-free green parts, such as the injection pressure, post-pressure, injection speed, packing time or mould temperature. Error! Reference source not found. shows these main injection parameters. The temperature of the feedstock was maintained below $185 \text{ }^\circ\text{C}$ to prevent the decomposition of the paraffin wax. Fig. S2a displays the progressive filling of the piece mould. The injection volume was further increased until constant weight of the pieces. Finally, a post-pressure scheme was applied aiming to prevent

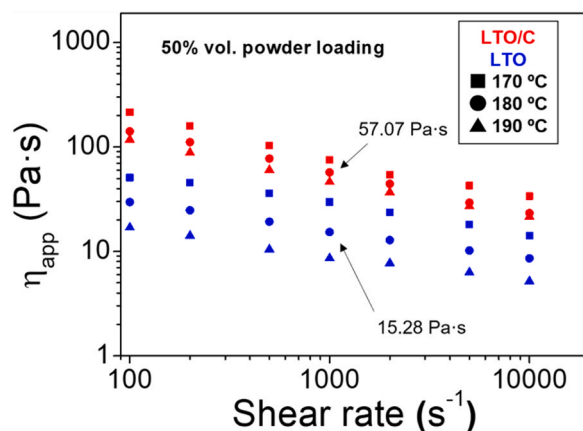


Fig. 4. Apparent viscosity against shear rate results for the feedstocks with 50% vol. LTO and 50% vol. LTO/C.

contraction of the pieces while cooling. The average dimensions of the injected disks were $11.97 \pm 0.05 \text{ mm}$ in diameter and $0.71 \pm 0.02 \text{ mm}$ in thickness (errors in dimensions correspond to the standard deviation of 10 injected samples).

3.4. Debinding and sintering

The injected pieces were subjected to a combined solvent and thermal debinding to remove the organic compounds. In the first step (solvent), the paraffin wax (PW) and the stearic acid (SA) were extracted by immersing the samples in an exceeding volume of n-heptane, at $50 \text{ }^\circ\text{C}$. Fig. 5a shows the amount of PW and SA that was removed over the leaching time. This is a typical behaviour [33,34]. The kinetics of this process were studied using the model proposed by Shivashankar and German [35], where the extraction happens in two steps. First, a quick dissolution of the most accessible binding system, and afterwards a slower penetration of the solvent in the inner parts of the sample and extraction of the non-polar components. Both follow this empiric relation:

$$\ln \frac{1}{F} = \frac{D_e t \pi^2}{\psi^2} + K$$

F is the fraction of binder still not dissolved, t is the time passed since the beginning of the solvent debinding, K is a constant for a powder-polymer system, D_e is the interdiffusion coefficient between polymer and ψ is the effective length scale, which for a cylindrical piece corresponds to:

$$\psi = \frac{\pi D^2 H / 4}{\pi D (H + D / 2)}$$

Where H is the height of the piece and D is the diameter. Thus, ψ value for the samples of this work is $3.16 \cdot 10^{-2} \text{ cm}$.

As it can be seen in Fig. 5a, the PW and SA are quickly removed from the parts within the first hour, reaching values approximately 95% of their theoretical amount. The study of the interdiffusion coefficient presented in Fig. 5b is in agreement with the two-step extraction: for the first one, D_{e1} is $3.66 \cdot 10^{-7} \text{ cm}^2 \cdot \text{s}^{-1}$; for the second one, D_{e2} is $1.36 \cdot 10^{-8} \text{ cm}^2 \cdot \text{s}^{-1}$. D_{e1} is 27 times greater than D_{e2} , which is, kinetically, a coherent result, because the initial process happens on the surface of the piece, where the n-heptane is abundant, and the concentration gradients of dissolved PW and SA are rapidly regulated. On the other hand, inside the piece these gradients cannot be rapidly readjusted due to limited accessibility and, as a result this process is slower. To conclude the solvent debinding studies, differential scanning calorimetry was performed on the samples before immersion and after 4 h immersed in n-heptane at $50 \text{ }^\circ\text{C}$. The DSC curves (Fig. S3) highlight that the solvent-debinded samples do not present the melting heat flow peaks corresponding to PW and SA, but still contain PP. The paraffin wax influence on the polypropylene melting point can be appreciated, as in the green part this temperature is lower than usual, an effect which has already been noticed in the literature on blends of PW and polyolefins [36,37].

The polypropylene was removed with the thermal debinding and, finally, the brown parts were sintered at $900 \text{ }^\circ\text{C}$ to increase the mechanical stability of the ceramic electrodes. These disk-type pieces have a diameter of $11.2 \pm 0.2 \text{ mm}$, a thickness of $0.65 \pm 0.01 \text{ mm}$, and a volume of 79.5% of the green parts as a result. Through the Archimedes method, their density was found to be $2.56 \pm 0.09 \text{ g}\cdot\text{cm}^{-3}$, resulting in a relative density of 74.3% and a porosity of 25.7%, based on a measured pycnometric density of LTO/C of $3.443 \pm 0.001 \text{ g}\cdot\text{cm}^{-3}$. Also, the X-ray diffraction analysis proved that no changes in the crystalline lattice of LTO occurred as result of the processing (Fig. S4).

Fig. 6 shows a comparison of the microstructure of green (a), brown (b), and sintered (c) parts. The polymeric component is distinguishable in the image as a dark-grey contrast in the BSE (backscattered electron) image, because of the lower molecular weight of the polymeric part

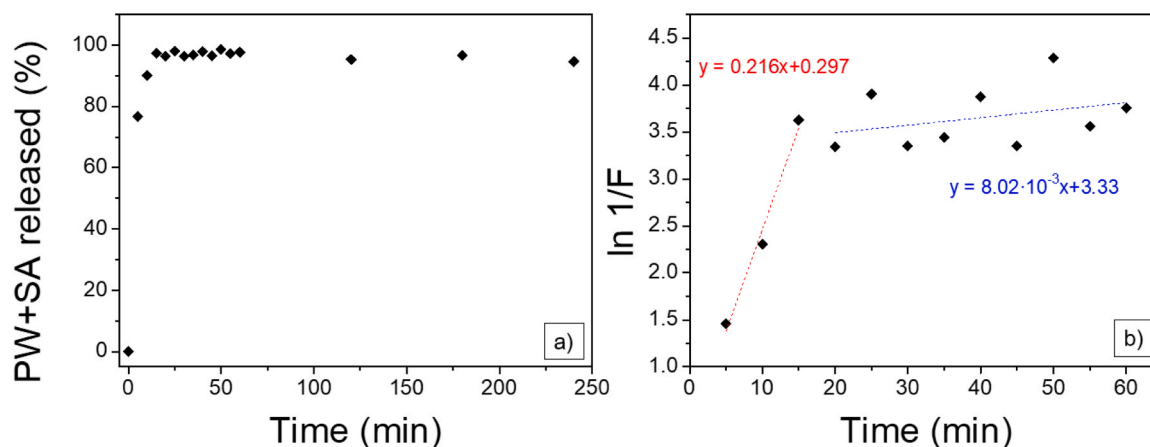


Fig. 5. a) Removal of paraffin wax and stearic acid of a green part immersed in n-heptane at 50 °C vs time, b) associated graph of $\ln 1/F$ (fraction of binder non solved) vs time.

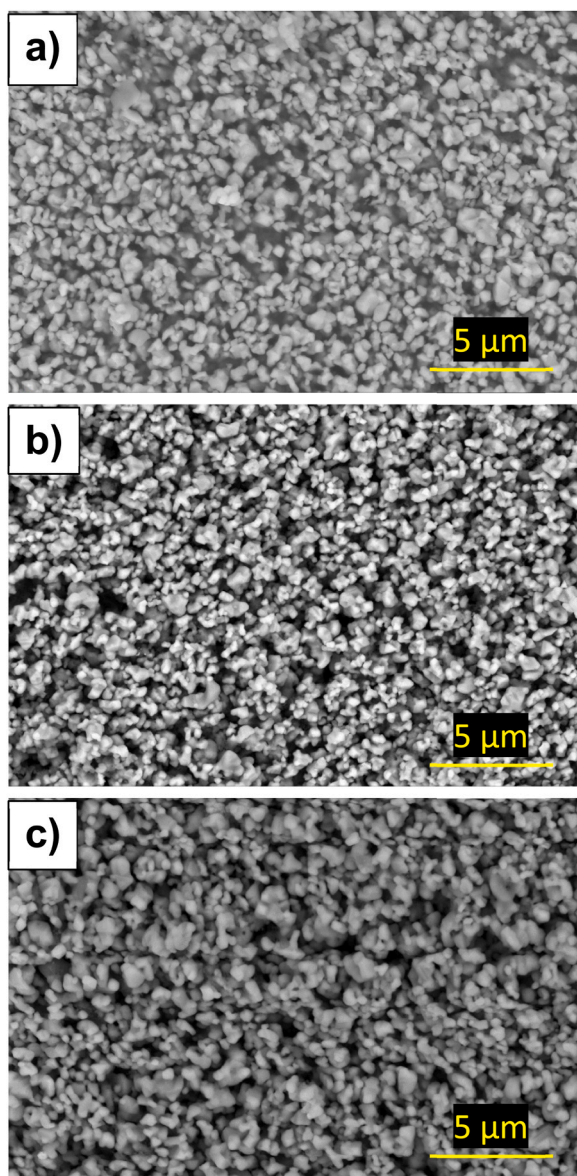


Fig. 6. Backscattered electrons mode scanning electron microscopy images of LTO/C surface of the parts for the stages: a) green, b) brown, c) sintered.

compared to the ceramic particles. In the brown part, no traces of binder are found, indicating the successful debinding process. In the sintered part, the typical porosity reduction and grain growth are not observed, due to the low sintering temperature used. This result is preferred, since the electrodes should be porous rather than compact to have a larger electrode-to-electrolyte surface area ratio.

According to elemental analysis tests performed on sintered parts the carbon content was determined to be $2.26 \pm 0.01\%$. This value is somewhat higher than the expected one, and this can find an explanation in the previous work of Sotomayor et al. [8] where, for a LTO processed by powder extrusion moulding, the reducing atmospheres of the thermal debinding and the sintering led to an inorganic carbon layer. According to Jung et al. [38], a carbon coating can actually help to improve the conductivity of lithium titanate, which is one of the main concerns in sintered LTO. Through transmission electron microscopy, the presence of this layer is confirmed, as it can be seen on the outer surface of an LTO crystalline particle, where an amorphous structure can be clearly identified (Fig. 7c). The surface carbon coating seems to adhere well to LTO as seen in Fig. 7b).

The conductivity of the samples was determined by impedance spectroscopy. For comparison, these were also performed on a reference sample of commercial LTO, without added carbon, which was uniaxially compacted and sintered in air at the same temperature and heating rate (same thermal treatment) as the LTO/C. The conductivity value of $7.7 (\pm 0.1) \cdot 10^{-9} \text{ S}\cdot\text{cm}^{-1}$ at 0.1 Hz of pure LTO corresponds to that of a typical insulator. This conductivity value is significantly improved by 1.5 orders of magnitude in the sintered LTO/C material with $2.8 (\pm 0.1) \cdot 10^{-7} \text{ S}\cdot\text{cm}^{-1}$, (see Fig. S5). Therefore, the addition of carbon black improves the conductivity of pristine LTO.

The electrochemical performance of the sintered LTO/C was evaluated by means of galvanostatic cycling with potential limitation. Inside a pouch-bag cell, metallic lithium was used as the counter-electrode, along with a glass fibre separator and commercial LP30 as the electrolyte. The first two cycles were programmed at a C/24 rate, and from then on, a higher C-rate of C/12 was used. This protocol ensured a stabilization of the system at the beginning of the experiment. Specifically, to allow for a proper wetting of the very thick electrode. The notoriously large areal mass loading of active material for the PIM processed parts ($\sim 166 \text{ mg}\cdot\text{cm}^{-2}$) required this consideration, as the amount of Li to be intercalated and de-intercalated is considerably higher than in conventional tape-casted electrodes, whose thickness are usually a few dozens of microns and their areal loadings between 25 and 35 $\text{mg}\cdot\text{cm}^{-2}$ [39]. The capacity of the cell for the first discharge was $155 \text{ mA}\cdot\text{h}\cdot\text{g}^{-1}$, close to the theoretical value of $175 \text{ mA}\cdot\text{h}\cdot\text{g}^{-1}$, but the volumetric and areal capacity are remarkably higher, $397 \text{ mA}\cdot\text{h}\cdot\text{cm}^{-3}$ and $25.8 \text{ mA}\cdot\text{h}\cdot\text{cm}^{-2}$ respectively. Sotomayor et al. [8] had already developed thick LTO

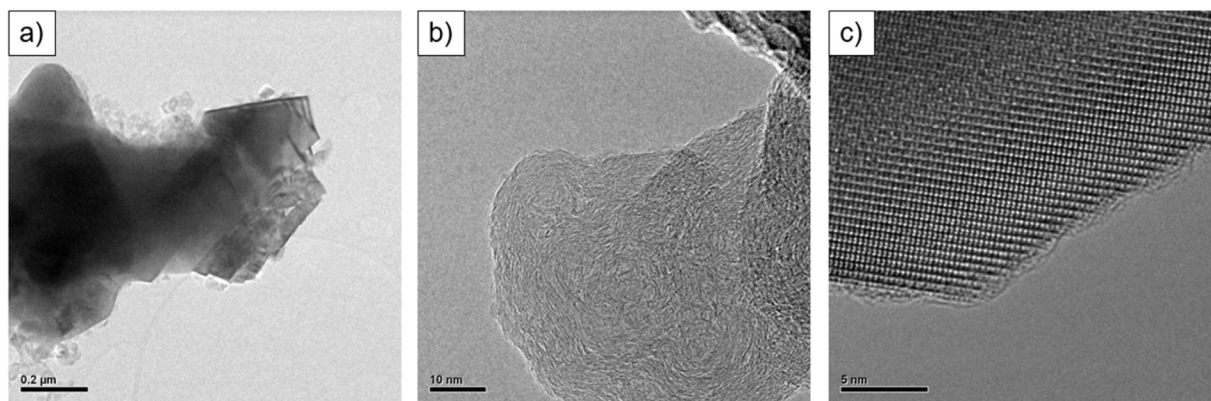


Fig. 7. TEM images of a) a grain of sintered LTO/C, b) an adhered carbon black grain, c) LTO covered by a carbon layer.

electrodes by powder extrusion moulding with a volumetric capacity ($319 \text{ mA}\cdot\text{h}\cdot\text{cm}^{-3}$) 3 times higher than a conventional tape-casted LTO; and one order of magnitude larger areal capacity ($15.2 \text{ mA}\cdot\text{h}\cdot\text{cm}^{-2}$). For the first cycle, PIM ceramic electrodes have even better volumetric and areal capacities than those obtained by PEM as indicated by the higher specific capacity of the former electrodes. This can be related to their greater porosity (25.7% versus 17%), which translates to a larger electrode/electrolyte contact surface facilitating the lithium exchange. The areal capacity improvement can be attributed as well to their greater thickness ($650 \mu\text{m}$ versus $475 \mu\text{m}$). In relation to cyclability, the cell underwent more than 20 cycles at C/12 rate, and despite still working appropriately, capacity fading was observed as it can be seen in Fig. 8. At the 25th cycle, the discharge capacity was $77 \text{ mA}\cdot\text{h}\cdot\text{g}^{-1}$. This pronounced capacity fading could be attributed to: (i) the partial polarization of the electrode, where the lithium ions are not fully deintercalated throughout the LTO sample at the charging process. The reason behind this could be their long diffusion path towards the electrode-electrolyte interphase, which could be dealt with larger porosities ensuring a good electrode-electrolyte contact; (ii) although rather unlikely, the formation of an extensive SEI that consumes some of the lithium which can be the counter ion to recently formed alkylcarbonates, as previously reported [19]; and (iii) to the lithium metal anode's inability to accommodate the high current densities and total capacities that result from using thick sintered electrodes. Besides, the excess amount of Li (30 mg, capacity ratio to LTO/C 5:1), and the electrolyte is actually attenuating the capacity fading, as stated before by Robinson et al. [40], who also prove that a full cell configuration with two intercalation electrodes would benefit the cyclability of thick

electrodes and paves the way for the potential use of these high density electrodes.

Still, even with those low values of specific capacity, they outperform LTO tape-casted ceramic sintered electrodes in terms of volumetric capacity. The reducing sintering atmosphere also has a positive effect in these performances, as previously stated with PEM-produced LTO [8], with tape-casted thick LTO [41] and with a LTO used for a semi-solid flow battery [22]. The presence of Ti^{3+} as a result of the sintering process, under a reducing atmosphere, can explain the seemingly odd initial step of the first discharge. This plateau over 1.5 V is not observed again in later cycles, and can be considered a sign of all of the titanium returning to the (IV) oxidation state after the first charge. These results are to be considered an intermediate step in the research that proves that ultra-thick LTO/C electrodes processed by PIM are an option to develop high-capacity batteries.

4. Conclusions

For the first time, thick electrodes of LTO including 2 wt% conductive carbon have been processed through powder injection moulding technique. This technology is easily scalable to industrial scale, and currently it is used in the manufacturing of ceramic and metallic parts. Starting from the ceramic powders and a previously defined binder composed of polypropylene, paraffin wax and stearic acid; torque and rheology studies suggested that a 50% volumetric ceramic powder charge was appropriate for injection. Using this technique, defect-free disk-type green parts were produced, and these were subsequently subject to solvent debinding, thermal debinding and sintering to

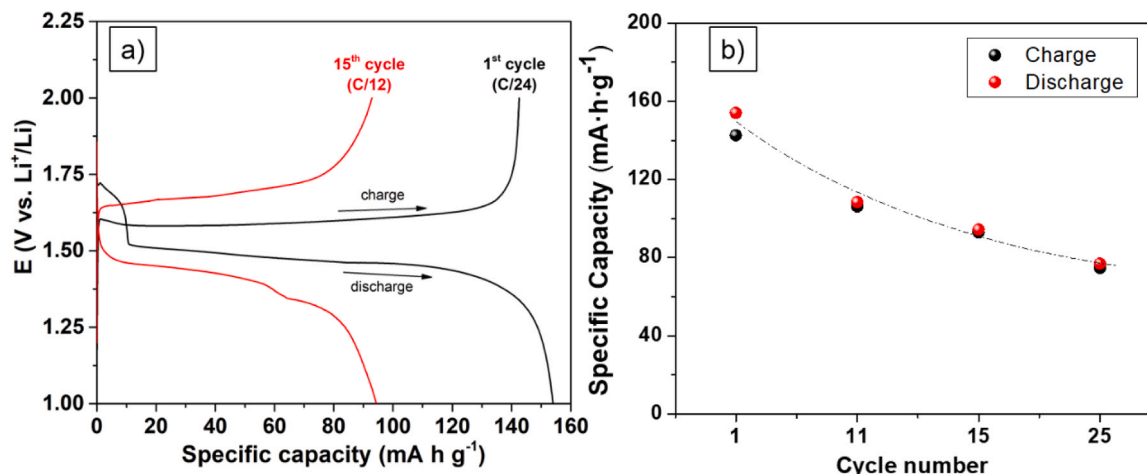


Fig. 8. a) Potential of the PIM LTO/C electrode versus specific capacity. b) Variation of the charge and discharge capacities of the electrode through the cycles.

produce solvent-free ceramic electrodes. Although the binder is successfully removed, the use of a controlled atmosphere during debinding and sintering allowed the parts to retain inorganic carbon from the decomposition of organic compounds. EIS analysis suggested that this conductive carbon can lead to an increase of conductivity of 1.5 orders of magnitude compared to similarly processed LTO without carbon. In a pouch-bag cell, these electrodes were capable of cycling against metallic lithium at C/24 and C/12 rates, and offered high values of volumetric and areal capacities, up to 403 mA·h·cm⁻³ and 26.0 mA·h·cm⁻², respectively. These values are slightly higher than those obtained for LTO samples obtained by Powder Extrusion Moulding. The results make LTO/C an interesting anodic material and highlight the potential of PIM as a technique for processing lithium-ion batteries electrode components.

Declaration of Competing Interest

The authors declare that they have no known competing financial interests or personal relationships that could have appeared to influence the work reported in this paper.

Data Availability

Data is available from the authors upon request.

Acknowledgements

The authors would like to thank the Agencia Española de Investigación/Fondo Europeo de Desarrollo Regional (FEDER/UE) MCIN/AEI/ 10.13039/501100011033 (projects PID2019–106662RBC43 and PID2022-140373OB-I00, and Madrid Government (Comunidad de Madrid-Spain) (DROMADER-CM (Y2020/NMT6584)) for funding. I. Romero-García thanks the Ministerio de Universidades (Spain, 25), and C. de la Torre-Gamarrá for fruitful discussion. All HIU authors express their gratitude to Helmholtz Association for the basic funding.

Funding for APC: Universidad Carlos III de Madrid (Read & Publish Agreement CRUE-CSIC 2023)

Appendix A. Supporting information

Supplementary data associated with this article can be found in the online version at [doi:10.1016/j.jeurceramsoc.2023.09.030](https://doi.org/10.1016/j.jeurceramsoc.2023.09.030).

References

- [1] B. Dunn, H. Kamath, J.-M. Tarascon, Electrical energy storage for the grid: a battery of choices, *Science* vol. 334 (80) (2011) 928–936.
- [2] V. Etacheri, R. Marom, R. Elazari, G. Salitra, D. Aurbach, Challenges in the development of advanced Li-ion batteries: a review, *Energy Environ. Sci.* vol. 4 (2011) 3243–3262.
- [3] M. Armand and J. Tarascon, “Building better batteries,” vol. 451, no. February, pp. 651–657, 2008.
- [4] Y. Liu, R. Zhang, J. Wang, Y. Wang, Current and future lithium-ion battery manufacturing, *ISCIENCE* vol. 24 (4) (2021), 102332.
- [5] L. Leira, H.L. Tiltse, A. Svendsen, K. Vetlesen, Irritant Cutaneous Reactions to N-methyl-2-pyrrolidone (NMP), *Contact Dermat.* vol. 27 (1992) 148–150.
- [6] V. Haufroid, et al., Biological monitoring and health effects of low-level exposure to N-methyl-2-pyrrolidone: a cross-sectional study, *Int. Arch. Occup. Environ. Heal.* vol. 87 (2014) 663–674.
- [7] D.L. Wood, J. Li, C. Daniel, Prospects for reducing the processing cost of lithium ion batteries, *J. Power Sources* vol. 275 (2015) 234–242.
- [8] M.E. Sotomayor, et al., Additive-free Li₄Ti₅O₁₂ thick electrodes for Li-ion batteries with high electrochemical performance, *J. Mater. Chem. A* vol. 6 (14) (2018) 5952–5961.
- [9] C. De la Torre-Gamarrá, et al., High mass loading additive-free LiFePO₄ cathodes with 500 μm thickness for high areal capacity Li-ion batteries, *J. Power Sources* vol. 458 (February) (2020).
- [10] R. Asthana, A. Kumar, N.B. Dahotre, Powder metallurgy and ceramic forming, crystalline ceramics and glasses, in: E. Lof (Ed.), *Materials Processing and Manufacturing Science*, Elsevier B.V., 2006, pp. 188–197.
- [11] R. German, A. Bose, *Injection Molding of Metals and Ceramics*, Metal Powder Industries Federation, Princeton, NJ, 1997.
- [12] B. Hausnerova, Powder injection moulding – an alternative processing method for automotive items, in: M. Chiaberge (Ed.), *New Trends and Developments in Automotive System Engineering*, InTech, Rijeka, Croatia, 2009, pp. 129–145.
- [13] P. Thomas-Vielma, A. Cervera, B. Levenfeld, A. Várez, Production of alumina parts by powder injection molding with a binder system based on high density polyethylene, *J. Eur. Ceram. Soc.* vol. 28 (2008) 763–771.
- [14] T. Jardiel, M.E. Sotomayor, B. Levenfeld, A. Várez, Optimization of the processing of 8-YSZ powder by powder injection molding for SOFC electrolytes, *Int. J. Appl. Ceram. Technol.* vol. 581 (2008) 574–581.
- [15] A.K. Panahi, H. Khoshkish, Fabrication of porous Ni – YSZ anodes by PSH-PIM, *Ionics (Kiel.)* vol. 17 (2011) 733–740.
- [16] J. Xiao, et al., Effect of pre-calcined ceramic powders at different temperatures on Ni-YSZ anode-supported SOFC cell / stack by low pressure injection molding, *Ceram. Int.* vol. 45 (16) (2019) 20066–20072.
- [17] G. Zhu, Y. Wang, Y. Xia, Environmental Science Ti-based compounds as anode materials for Li-ion batteries, *Energy Environ. Sci.* vol. 5 (2012) 6652–6667.
- [18] T.-F. Yi, H. Liu, Y. Zhu, L. Jiang, Y. Xie, R. Zhu, Improving the high rate performance of Li₄Ti₅O₁₂ through divalent zinc substitution, *J. Power Sources* vol. 215 (2012) 258–265.
- [19] C.J. Jafta, et al., “Probing the Li₄Ti₅O₁₂ interface upon lithium uptake by operando small angle neutron scattering, *ChemSusChem* vol. 13 (2020) 3654–3661.
- [20] T.F. Yi, S.Y. Yang, Y. Xie, Recent advances of Li₄Ti₅O₁₂ as a promising next generation anode material for high power lithium-ion batteries, *J. Mater. Chem. A* vol. 3 (11) (2015) 5750–5777.
- [21] C. Cai, et al., Thick sintered electrode lithium-ion battery discharge simulations: incorporating lithiation-dependent electronic conductivity and lithiation gradient due to charge cycle, *J. Electrochem. Soc.* vol. 167 (no.) (2020), 140542.
- [22] E. Ventosa, M. Skoumal, J. Vazquez, C. Flox, J. Arbiol, Electron Bottleneck in the charge / discharge mechanism of lithium titanates for batteries, *ChemSusChem* vol. 8 (2015) 1737–1744.
- [23] W. Meng, B. Yan, Y. Xu, Scalable synthesis of Ti³⁺ self-doped Li₄Ti₅O₁₂ microparticles as an improved performance anode material for Li-ion batteries, *J. Alloy. Compd.* vol. 788 (2019) 21–29.
- [24] Y. Kuo, J. Lin, *Electrochimica Acta* One-pot sol-gel synthesis of Li₄Ti₅O₁₂ / C anode materials for high-performance Li-ion batteries, *Electrochim. Acta* vol. 142 (2014) 43–50.
- [25] L. Cheng, X. Li, H. Liu, H. Xiong, P. Zhang, Carbon-Coated Li₄Ti₅O₁₂ as a high rate electrode material for Li-Ion intercalation, *J. Electrochem. Soc.* vol. 154 (7) (2007) 692–697.
- [26] A. Subhan, F. Oemry, S.N. Khusna, E. Hastuti, Effects of activated carbon treatment on Li₄Ti₅O₁₂ anode material synthesis for lithium-ion batteries, *Ionics (Kiel.)* vol. 25 (2019) 1025–1034.
- [27] J. Man, et al., Fabrication of micro-sized piezoelectric structure using powder injection molding with separated mold system, *Ceram. Int.* vol. 44 (11) (2018) 12709–12716.
- [28] I. Manas-Zloczower. *Mixing and Compounding of Polymers Theory and Practice*, Second ed., Hanser, Munich, 2009.
- [29] D. Ostwald, Ueber die Geschwindigkeitsfunktion der Viskosität disperser Systeme. I, *Kolloid-Z.* vol. 36 (1925) 99–128.
- [30] A. De Waele, Viscometry and plastimetry, *J. Oil Colour. Chem. Assoc.* vol. 6 (1923) 33–69.
- [31] M.J. Edirisinghe, H.M. Shaw, K.L. Tomkins, Flow behaviour of ceramic injection moulding suspensions, *Ceram. Int.* vol. 18 (3) (1992) 193–200.
- [32] M.J. Edirisinghe, J.R.G. Evans, Properties of ceramic injection moulding formulations, *J. Mater. Sci.* vol. 22 (1987) 269–277.
- [33] S. Eroglu, H.I. Bakan, Solvent debinding kinetics and sintered properties of injection moulded 316L stainless steel powder, *Powder Met.* vol. 48 (4) (2005) 329–332.
- [34] M.E. Sotomayor, B. Levenfeld, A. Várez, Powder injection moulding of premixed ferritic and austenitic stainless steel powders, *Mater. Sci. Eng. A* vol. 528 (9) (2011) 3480–3488.
- [35] T.S. Shivashankar, R.M. German, Effective length scale for predicting solvent-debinding times of components produced by powder injection molding, *J. Am. Ceram. Soc.* vol. 82 (5) (2004) 1146–1152.
- [36] I. Krupa, A.S. Luyt, Thermal properties of polypropylene / wax blends, *Thermochim. Acta* vol. 372 (2001) 137–141.
- [37] M.E. Sotomayor, I. Krupa, A. Várez, B. Levenfeld, Thermal and mechanical characterization of injection moulded high density polyethylene / parafin wax blends as phase change materials, *Renew. Energy* vol. 68 (2014) 140–145.
- [38] H. Jung, J. Kim, B. Scrosati, Y. Sun, Micron-sized, carbon-coated Li₄Ti₅O₁₂ as high power anode material for advanced lithium batteries, *J. Power Sources* vol. 196 (18) (2011) 7763–7766.
- [39] M.A. Ghadkolai, S. Creager, J. Nanda, R.K. Bordia, Freeze tape cast thick molybdenum doped Li₄Ti₅O₁₂ electrodes for lithium-ion batteries, *J. Electrochem. Soc.* vol. 164 (12) (2017) A2603–A2610.
- [40] J. Pierce Robinson, J.J. Ruppert, H. Dong, G.M. Koenig, Sintered electrode full cells for high energy density lithium-ion batteries, *J. Appl. Electrochem.* vol. 48 (11) (2018) 1297–1304.
- [41] C. de la Torre-Gamarrá, et al., Tape casting manufacturing of thick Li₄Ti₅O₁₂ ceramic electrodes with high areal capacity for lithium-ion batteries, *J. Eur. Ceram. Soc.* vol. 41 (1) (2021) 1025–1032.